Natural Resources for Human Health
eISSN: 2583-1194

Original Research

Received 29 May 2026
Revised 21 June 2026
Accepted 18 July 2026

Natural Resources for Human Health 2026, Vol. 6 (9s): 1143–1156

KEYWORDS:
breast cancer; contrast-enhanced mammography; molecular subtype; calcification; mammographic mass; cross-sectional study; CMMD

Association of Contrast-Enhanced Mammography Imaging Features with Molecular Subtypes of Breast Cancer: A Cross-Sectional Study

Wael Ahmed Maher Mostafa ElHik[1], Hesham Wageh Ezzat Abd Rabbo [2], Ahmed Mudkhre Shareef[3], Mohamed Abd El Aal Ali Osman[4], Saba Mahdi Jasim[5], Mohammad Alzreiqat[6], Mohamed Ahmed Soliman[7]

[1]Department of Radiology, Faculty of Medicine, Ain Shams University, Cairo, Egypt.
Email: Wael.maher@gmail.com | ORCID: 0009-0002-2920-8596
[2]General Surgery Department, Faculty of Medicine, Fayoum University, Fayoum, Egypt.
Email: Hwe00@fayoum.edu.eg | ORCID: 0009-0001-1552-3651
[3]Department of Radiology, College of Medicine, Ninevah University, Mosul, Nineveh, Iraq.Email: ahmed.shareef@uoninevah.edu.iq | ORCID: 0000-0002-9851-5664
[4]Department of General Surgery, Endoscopy and Surgical Oncology, Sohag University, Sohag, Egypt.
Email: Mohamed.abdelaal@med.sohag.edu.eg | ORCID: 0009-0005-3555-4905
[5]Oncology Teaching Hospital, Medical City, Baghdad, Iraq.
Email: sabamj.onco@gmail.com | ORCID: 0009-0005-8988-0618
[6]School of Medicine, The University of Jordan, Amman, Jordan.
Email: mohammadalzreiqat78@gmail.com | ORCID: 0009-0003-3748-5232
[7]Department of Radiology, Faculty of Medicine, Beni-Suef University, Beni-Suef, Egypt.
Email: d.msoliman2015@gmail.com | ORCID: 0009-0006-0975-5292

ABSTRACT:

Background: Breast cancer molecular subtypes differ biologically and may exhibit distinct imaging phenotypes. This study examined whether mammographic morphologic features corresponding to the low-energy structural component of contrast-enhanced mammography (CEM) were associated with molecular subtype.

Methods: A retrospective cross-sectional secondary analysis was conducted using the molecular-subtype branch of the Chinese Mammography Database. The patient-level cohort included 749 malignant cases classified as luminal A, luminal B, HER2-enriched, or triple-negative. Mass-only, calcification-only, and combined mass-with-calcification presentations were compared using Pearson's chi-square test and Cramer's V. Multinomial logistic regression adjusted for age and breast laterality. Prespecified secondary contrasts used modified Poisson regression with robust variance.

Results: The cohort included 152 luminal A, 376 luminal B, 135 HER2-enriched, and 86 triple-negative cancers. Morphologic feature distribution differed across subtypes (chi-square[6] = 52.72, P < .001; Cramer's V = .188, 95% bootstrap CI [.150, .242]). Calcification-containing presentations occurred in 68.9% of HER2-enriched cancers, whereas 75.6% of triple-negative cancers were mass-only. Relative to luminal A and mass-only presentation, HER2-enriched cancer was associated with mass plus calcification (adjusted relative risk ratio [RRR] = 3.72, 95% CI [2.16, 6.41]) and calcification only (RRR

= 3.85, 95% CI [1.93, 7.68]). Secondary analyses confirmed higher HER2-enriched prevalence with calcification-containing presentation and higher triple-negative prevalence with mass-only presentation.

Conclusion: Simple structural mammographic features were associated with breast cancer molecular subtype. These findings support a subtype-related low-energy morphologic signal relevant to CEM interpretation, but they do not address contrast enhancement and cannot replace pathological receptor testing.

INTRODUCTION

Breast cancer is a significant health issue, and the most common cancer in women worldwide. It is estimated that there were around 2.3 million new cases of female breast cancer and 666,000 deaths from the cancer in 2022, accounting for 11.6% of all new cancer diagnoses and 6.9% of all cancer deaths (Bray et al., 2024). The clinical importance of incidence is further compounded by the biological heterogeneity of breast cancer; that is, tumours of the same size or morphology may have different natural histories, treatment sensitivities and prognosis (Harbeck et al., 2019; Johnson et al., 2021). Thus, accurate characterization should be achieved by combining the imaging information with pathological and molecular information and not only on the basis of anatomic appearance.

Immunohistochemical expression of estrogen receptor (ER), progesterone receptor (PR), human epidermal growth factor receptor 2 (HER2) and the proliferation marker Ki-67 is used as a way of approximating clinically relevant molecular phenotypes in routine practice. Although these markers do aid in classification into luminal A, luminal B, HER2-enriched and triple-negative breast cancer (TNBC), the classifications do not match exactly with the intrinsic classifications in the gene-expression-defined intrinsic subtypes (Prat et al., 2015; Tang & Tse, 2016). However, the categories also have direct clinical implications as they help with endocrine treatment, HER2-directed therapy, the choice of chemotherapy, and prognosis (Harbeck et al., 2019; Johnson et al., 2021). Preoperative imaging characteristics that correlate with these categories might be useful as additional information about whole-tumor phenotype and help to interpret imaging-pathology discordance.

In contrast-enhanced mammography (CEM), both the high-resolution mammographic morphology and the information associated with the uptake of iodinated contrast are used. A standard exam produces two views–a craniocaudal (CC) and a mediolateral oblique (MLO)–with two images each: a low-energy image that looks like a conventional 2D mammogram, and a recombined image that highlights enhancement associated with tumor vascularity (Covington et al., 2024; Jochelson & Lobbes, 2021). Low-energy CEM images have been reported to be diagnostic of conventional morphologic findings such as masses and calcifications, as compared to full-field digital mammography (Francescone et al., 2014). Comparative studies also have shown that for certain clinical scenarios, the use of recombined CEM can augment the detection of lesions or evaluation of disease extent compared to low-energy or standard 2D mammography (Phillips et al., 2023; Nguyen et al., 2024). CEM therefore could provide a pragmatic link between structural mammography and vascular imaging, but it does involve the administration of iodinated contrast and a slightly different imaging pathway as compared to conventional mammography (Covington et al., 2024; Polat et al., 2020).

There is increasing evidence that there are identifiable imaging phenotypes that reflect the biology of the breast cancer disease. Luminal tumors are sometimes referred to as irregular or spiculated, HER2-enriched cancers are sometimes associated with calcifications and lack of mass enhancement, and TNBC more often has a mass with oval or round morphology and relatively circumscribed margins (Johnson et al., 2021; Sohn et al., 2016; Wang et al., 2022). CEM studies have also found that there are differences in lesion size, enhancement heterogeneity, non-mass enhancement, rim enhancement and quantitative density/contrast ratio in different subtypes (Ma et al., 2025; Ping et al., 2026; Wang et al., 2022). There are also radiomics investigations which have shown that quantitative CEM texture patterns have the ability to discriminate TNBC and selected receptor-defined groups, but with varying performances across different cohorts, views, segmentation strategies and validation approaches (Marino et al., 2020; Nicosia et al., 2022; Zhang et al., 2021; Zhu et al., 2024).

However, evidence is still scarce due to the retrospective, single-center study design, small numbers of patients in certain subtypes, and varying definitions of features across studies, as well as limitations in patient-level CEM data access (Ma et al., 2025; Ping et al., 2026). The availability of open mammography resources labeled with molecular data allows investigation of

whether there is reproducible subtype information in the morphologic feature domain shared by conventional mammography and the low-energy component of CEM. The Chinese Mammography Database (CMMD) is especially valuable for this purpose, as it has biopsy-proven diagnosis and molecular subtypes for a specific patient population, thus it can be used for patient-level secondary analyses (Cai et al., 2023). On the other hand, since there are no post-contrast recombined CEM images in CMMD, it could be used for analysis of morphologic features as a low-energy equivalent, but could not be used for analysis of enhancement intensity, enhancement in the lesion, background parenchymal enhancement (BPE), and kinetic behavior.

This study aimed to investigate the relationship between mammographic morphologic characteristics that are important to the low-energy component of CEM, and breast cancer molecular subtypes utilizing patient-level CMMD data. In particular, the numbers of mass, calcification and combined mass/calcification presentations in the luminal A, luminal B, HER2-enriched and triple-negative cancers were compared, considering age and breast laterality. Molecular subtype was not considered initially as an independent variable in the primary hypothesis, which was that abnormality type would not be independent of molecular subtype. The directional hypotheses were that HER2-enriched cancers would be more likely to present with calcification compared to mass-only presentation and TNBC would be more likely to present with mass-only compared to calcification. The null hypothesis was that the distribution of these morphologic features would not vary between the molecular subtypes, once the measured covariates were considered.

LITERATURE REVIEW

The molecular classification of breast cancer was born out of the knowledge that breast cancer is made up of biologically distinct diseases, and not one clinicopathological entity. Luminal A, luminal B, HER2-enriched and triple-negative are the four most commonly used phenotypes in the contemporary clinical classification using ER, PR, HER2 and Ki-67 as surrogates (Prat et al., 2015; Tang & Tse, 2016). Luminal tumors are hormone receptor-positive and typically are treated with endocrine therapy, while HER2-positive tumors might benefit from HER2-directed therapy, and TNBC is hormone receptor-negative, HER2-negative, and is treated without endocrine or HER2-directed therapy (Harbeck et al., 2019; Johnson et al., 2021). Imaging can help provide more information on the whole lesion that was sampled but is not a substitute for pathological receptor testing, as a core biopsy may not sample a heterogeneous lesion (Harbeck et al., 2019; Zhang et al., 2021).

Well-known correlations exist between morphology and molecular phenotype in mammography, ultrasound and magnetic resonance imaging. Recurring patterns were noted in syntheses for breast radiologists: Luminal cancers were more likely to present as a spiculated irregular mass, HER2-enriched cancers were more likely to display calcifications or extensive disease and TNBCs were more likely to present as non-calcified masses with round or oval shapes and circumscribed or indistinct margins (Johnson et al., 2021; Sohn et al., 2016). These patterns are probabilistic and not diagnostic as there is significant overlap between the various patterns and the pattern depends on the size of the lesion, the histology grade, the density of the breast and the acquisition technique (Johnson et al., 2021). They can thus not be used for the definitive identification of the subtype, but for association testing and risk stratification.

CEM further extends this morphological approach with the generation of low-energy and recombined images. In contrast, the low-energy image retains the main structural information that is utilized in traditional mammography, like mass detection and the identification of calcifications, whereas the recombined images show contrast uptake after suppression of background fibroglandular tissue (Covington et al., 2024; Jochelson & Lobbes, 2021). Low-energy CEM images have been directly compared to routine full-field digital mammography (FFDM) and have been shown to be able to achieve image quality and depiction of lesion information similar to FFDM (Francescone et al., 2014). The morphologic domain of CEM is low-energy, and this overlap gives a technical justification for studying conventional mammographic morphology as a proxy for the low-energy morphologic domain of CEM but does not allow inference about post-contrast enhancement.

Wang et al. (2022) performed a retrospective study of 151 patients with 160 malignant lesions, and analyzed the qualitative and quantitative characteristics of CEM according to the molecular subtypes. Non-luminal lesions were larger and showed a higher variability in lesion density, and HER2-enriched cancers showed a higher percentage of calcifications and density variability. Selected size-normalized enhancement measurements were different for TNBC (Wang et al., 2022), and non-mass enhancement was independently associated. The study showed that the combination of morphology and quantitative enhancement is promising, although there were uncertainties with some of the estimates given the relatively small number of patients in the HER2-enriched and TNBC groups.

Later, more detailed, computer-generated CEM phenotyping efforts have taken place. In 367 pathologically confirmed cancers, Zhang et al. (2021) created radiomic models based on subtracted CEM images, and found that the craniocaudal and mediolateral oblique model combined had an area under the receiver operating characteristic curve of 0.90 in the test set for discriminating TNBC from non-TNBC. Radiomic features from recombined CEM images were also shown to have potential for identifying receptor-defined molecular groups in Nicosia et al. (2022). Zhu et al. (2024) confirmed this in a two-center cohort using external testing and discovered that in general, combined low-energy and recombined-image radiomics models performed better than their single-image counterparts, although the performance of the models differed based on the type of cancer. These findings corroborate the use of biological signal in CEM texture, but there are some differences in segmentation, feature selection, class balance, and external validation that prevent a direct comparison between studies (Nicosia et al., 2022; Zhang et al., 2021; Zhu et al., 2024). More recent investigations, involving semantic features, have gone beyond strictly one subtype. Ma et al. (2025) tested 241 patients and identified radiological characteristic features of CEM to differentiate between the three groups: luminal, HER2-enriched and triple-negative. For some of the binary subtype tasks, the performance of models combining low-energy and dual-energy subtraction features exceeded the performance obtained by either image type, indicating that structural and enhancement information are complementary (Ma et al., 2025). Ping et al. (2026) performed a 2026 study on 183 patients with a total of 195 lesions, in which differences in lesion size, morphology, enhancement pattern, time-gray curve type and microcalcification frequency were identified between the different subtypes (HER2-overexpressing and TNBC more frequently presented as non-mass). Both studies demonstrate the value of morphology, and the value of enhancement-specific variables in providing information that is not available in conventional mammography. Even though conventional mammography is not a key aspect of molecular-phenotype research, it has a very important role to play, since it is readily available and because mass and calcification patterns are elements of CEM interpretation. The performance of mammographic radiomics in predicting molecular subtype has been moderate, while some recent deep-learning studies have attempted to combine images with clinical information to enhance subtype categorisation (Luo et al., 2025; Mota et al., 2024). These studies are generally about prediction, but if we want to ask a different question we might ask whether there is any systematic difference in the distribution of observable features between these groups of subtypes – this is an epidemiological association analysis. Even when classification models are created, association estimates, confidence intervals and effect sizes are still required, as performance of the predictive models does not explain the nature of the relationships between features and the subtypes. The CMMD was developed to overcome the lack of openly-available mammography data with biopsy confirmation and molecular subtype. It comprises 3712 mammograms from 1775 patients in two branches of which 1498 mammograms from 749 patients are in the molecular-subtype branch (Cai et al., 2023). The clinical file for each corresponding patient includes patient identifier, age, laterality, type of abnormality, malignancy classification and molecular subtype. It has the advantages of public accessibility, patient-level linkage, uniform core variables and a relatively large molecularly labeled population, but the disadvantages are that it is a single-country population, acquired as a retrospective population, has a coarse abnormality categorization, and lacks receptor-level values or CEM enhancement variables (Cai et al., 2023). The real question is not, therefore, whether or not CEM is able to show biologically relevant information but whether simple, reproducible morphologic features are still measurably associated with subtype in a relatively large open cohort. Showing such associations would lend support to the low-energy morphological aspect of the CEM hypothesis, and provide a clear starting point for future research using actual paired low-energy/recombined images. The absence of an association would also be useful because it would imply that association-specific (enhancement-specific) or higher dimensional radiomic features are required. The current analysis takes up this deficit with a cross-sectional approach that was prespecified and makes explicit the limits of inference to the morphologic features available in CMMD.

METHODOLOGY

Study Design and Reporting Framework

This study is a secondary analysis of a publicly available imaging dataset and was conducted as a retrospective cross-sectional analysis. There was no attempt to model the longitudinal outcome or follow-up time, and imaging features and molecular subtype were analyzed at the patient level for the same diagnostic episode. Reporting was conducted based on Strengthening the Reporting of Observational Studies in Epidemiology guidelines for cross-sectional studies (von Elm et al., 2007).

DATA SOURCE

The data were retrieved from the Chinese Mammography Database, which is freely available on The Cancer Imaging Archive and described by Cai et al. (2023). We obtained mammograms of patients from China who had breast imaging during the period July 2012 to January 2016. The whole database can be split up into two branches: a benign/malignant branch with biopsy-

confirmed diagnosis and a malignant branch with molecular subtype labels (Cai et al., 2023). The official revised clinical spreadsheet and its associated TCIA image manifest were used for analysis.

Study Population and Eligibility Criteria

Patients were identified from the source population in CMMD. Records were eligible if the record contained (1) a unique patient identifier in the molecular-subtype branch; (2) breast disease coded as malignant; (3) a molecular-subtype coded as "luminal A", "luminal B", "HER2-enriched" or "triple-negative" (TNBC); (4) complete age, laterality, and abnormality-type information; and (5) an associated mammographic examination. Records with no subtype information, benign disease, duplicate patients, or missing information about the primary variable were excluded. After revision, 749 subtype-labeled patient records were included in the file, with patients represented only once in the molecular-subtype branch, and the analytical unit was the patient, not the image or the mammographic view (Cai et al., 2023). This avoided the artificial increase in the number of images due to the craniocaudal and mediolateral oblique images.

Operational Definition of Imaging Features

The main imaging exposure was the type of CMMD abnormality (mass only, calcification only or mass and calcification). The laterality was coded as left or right. Post-contrast images and enhancement descriptors are not available in the database. Thus, the term CEM imaging features was translated to the conventional morphologic feature domain tested in the low-energy component of a CEM examination in this secondary analysis. The definition was chosen because the low-energy CEM images were shown to be similar to standard full-field digital mammograms for conventional lesion depiction (Francescone et al., 2014); however, the original CMMD images were not characterized as being contrast-enhanced images. Enhancement intensity, enhancement distribution, internal enhancement pattern, background parenchymal enhancement and kinetic variables were not included in the data set and were not inferred.

Outcome Definition

The four-level molecular subtype variable provided in CMMD (luminal A, luminal B, HER2-enriched or triple-negative) was the primary outcome. These labels were based on the original pathology-based classification of the source data set, and analysed without pathology-based re-classification from imaging appearance. Although clinical surrogate subtyping typically involves ER, PR, HER2 and Ki-67, the actual receptor measurements are not stored in the public clinical file and verification of the subtype labels (in terms of different thresholds) was therefore not possible (Cai et al., 2023; Tang & Tse, 2016).

Covariates and Potential Confounding

Age was included as a continuous covariate since there may be differences in imaging presentation and subtype distribution with age (Johnson et al., 2021). Laterality of the breast was kept as a prespecified adjustment variable and descriptive characteristic. A few other possible confounders, such as breast density, tumor size, histologic grade, menopausal status, and center were not available in the clinical spreadsheet and were not included in the analysis, despite the fact that they were considered when interpreting the adjusted associations.

Data Management and Quality Control

The clinical spreadsheet was imported without altering the original source spreadsheet. Only a separate analysis copy was created, and the variables were standardized in terms of abbreviating their names and the labels of the categories. Patient identifiers were validated for uniqueness and the number of eligible records was verified against the published description of the CMMD (Cai et al., 2023). Frequency tables were used to determine if labels were invalid, if there was any structural missingness, and if there were any unexpected values. Age was verified to make sure that it was within a reasonable range prior to modeling. No imputation was needed for any data as all 749 eligible patients had complete data for subtype, abnormality type, age and laterality. The manifest identified that the identifiers were associated with image records, and the clinical data being analyzed were de-identified.

Statistical Analysis

Clinical-pathological data were summarized for all patients and for each of the molecular subtypes. Age was summarized as mean and standard deviation and compared between subtypes with one-way analysis of variance (ANOVA) and, for distributional robustness, with the Kruskal-Wallis test. Values of categorical variables were reported in terms of percentages

and frequencies. Pearson's chi-square test of independence was used for the primary unadjusted analysis to compare the four molecular subtypes with respect to the abnormality type (three levels). Expected cell counts were considered prior to interpretation of the test. Cramer's V with a nonparametric 95% confidence interval (CI) obtained from 10,000 bootstrap resamples of the data was used to summarize the magnitude of the overall categorical association. To detect the cells that make the strongest contribution to the global association, the cells' standardized residuals were calculated. Baseline-category multinomial logistic regression was used to estimate adjusted associations (reference outcome: luminal A). Abnormality type was modeled as a categorical predictor, with mass-only presentation as the reference, and age (centered at the cohort mean and scaled per 10 years) and laterality as prespecified covariates. Results were reported as relative risk ratios (RRRs) with Huber-White sandwich 95% confidence intervals (CIs) for luminal B, HER2-enriched and triple-negative cancer compared to luminal A. A likelihood-ratio test was used to evaluate the overall contribution of abnormality type (full vs reduced models). The convergence of models was evaluated and sparse cells were checked for sparse-data instability or quasi-separation. Two clinically relevant secondary comparisons were assessed: HER2-enriched versus all other subtypes for presentation with calcification, and TNBC versus non-TNBC for presentation with mass alone. These analyses were based on the directionality of the hypotheses generated from previous imaging studies (Johnson et al., 2021; Wang et al., 2022). Since prevalence ratios (PRs) are more appropriate to directly estimate the relative prevalence for binary outcome data (Zou, 2004), modified Poisson regression with robust variance was used to estimate PRs. A false-discovery-rate (FDR) procedure (Benjamini-Hochberg) was used to control the two secondary P values. A sensitivity analysis was done in which the two luminal subtypes (luminal A and B) were grouped together into a single luminal group, and adjusted PRs were calculated for each type of abnormality compared to mass-only presentation. All tests were two-sided, and the level of significance (alpha) was set at .05. These provided exact P values, effect estimates and 95% confidence intervals. All analyses were conducted in Python 3.12.13 using the pandas, numpy and scipy libraries (versions 2.2.3, 2.3.5 and 1.17.0, respectively), while figures were created using matplotlib (version 3.10.8) and seaborn (version 0.13.2). The data were cross-sectional and observational and associations were not assumed to be causal.

Ethical Considerations and Data Availability

The analysis used an existing, publicly available, de-identified dataset and involved no direct participant contact or new intervention. The original data collection and de-identification procedures were documented by the dataset authors and TCIA (Cai et al., 2023). The need for additional institutional review should be confirmed according to the researcher's local policy before submission. To promote reproducibility, the dataset DOI, eligibility rules, variable recoding, software versions, and analysis specifications are reported in this manuscript.

RESULTS

Cohort Selection and Characteristics

The revised CMMD clinical file contained 1,872 records. Of these, 556 benign records were excluded, leaving 1,316 malignant records. A further 567 malignant records did not have a molecular subtype label. The final molecular-subtype branch therefore comprised 749 eligible patients, all of whom had complete age, laterality, abnormality-type, and subtype data. Patient identifiers were unique in this branch, and no patient-level duplicate required removal. The cohort-selection process is summarized in Figure 1.

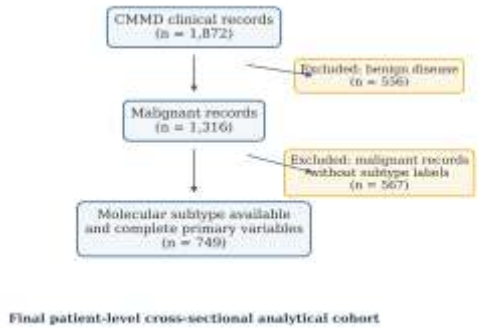

Figure 1 Selection of the Patient-Level Analytical Cohort

The mean age of the analytical cohort was 49.8 years (SD = 10.8; median = 49; interquartile range, 43-57; range, 21-87). Luminal B was the most frequent subtype (n = 376, 50.2%), followed by luminal A (n = 152, 20.3%), HER2-enriched (n = 135, 18.0%), and triple-negative cancer (n = 86, 11.5%). In 385 patients (51.4%) the left breast was involved. There were no significant differences in age among the groups of subtypes (F[3, 745] = 1.75, P = .155) and the Kruskal-Wallis analysis (H = 5.47, P = .140) confirmed this. However, there was no relationship between laterality and subtype (chi-square[3] = 3.77, P = .288).

Table 1 Patient Characteristics Overall and by Molecular Subtype

Characteristic	Overall (N = 749)	Luminal A (n = 152)	Luminal B (n = 376)	HER2-enriched (n = 135)	Triple-negative (n = 86)	P
Age, years, mean (SD)	49.8 (10.8)	51.4 (11.2)	49.3 (10.8)	50.2 (10.2)	48.7 (10.8)	.155
Left breast, n (%)	385 (51.4)	81 (53.3)	181 (48.1)	73 (54.1)	50 (58.1)	.288
Right breast, n (%)	364 (48.6)	71 (46.7)	195 (51.9)	62 (45.9)	36 (41.9)	

Note. P value for age is from one-way analysis of variance; the laterality P value is from Pearson's chi-square test. SD = standard deviation.

Distribution of Morphologic Features

The most frequent morphologic form was mass-only presentation (55.7%, n = 417) followed by mass with calcification (31.2%, n = 234) and calcification-only presentation (13.1%, n = 98). There was a significant difference in the distribution between the molecular subtypes (Table 2). The percentage of luminal A, luminal B, HER2-enriched and triple-negative cancers presenting as mass-only was 63.2%, 56.9%, 31.1% and 75.6%, respectively. 68.9% of HER2-enriched cancers, on the other hand, had calcification, with 23.0% having only calcification and 45.9% having both a mass and calcification. These within-subtype distributions are shown in Figure 2. For clinical context, representative published CEM cases illustrating the calcification-containing HER2-enriched phenotype and the mass-dominant triple-negative phenotype are presented in Figure 3 (Ferenčaba et al., 2026).

Table 2 Mammographic Morphologic Features by Molecular Subtype

Molecular subtype	Mass only, n (%)	Calcification only, n (%)	Mass with calcification, n (%)	Total, n
Luminal A	96 (63.2)	18 (11.8)	38 (25.0)	152
Luminal B	214 (56.9)	42 (11.2)	120 (31.9)	376
HER2-enriched	42 (31.1)	31 (23.0)	62 (45.9)	135
Triple-negative	65 (75.6)	7 (8.1)	14 (16.3)	86
Overall	417 (55.7)	98 (13.1)	234 (31.2)	749

Note. Percentages in subtype rows are calculated within molecular subtype. Pearson's chi-square(6) = 52.72, P < .001; Cramer's V = .188, 95% bootstrap CI [.150, .242].

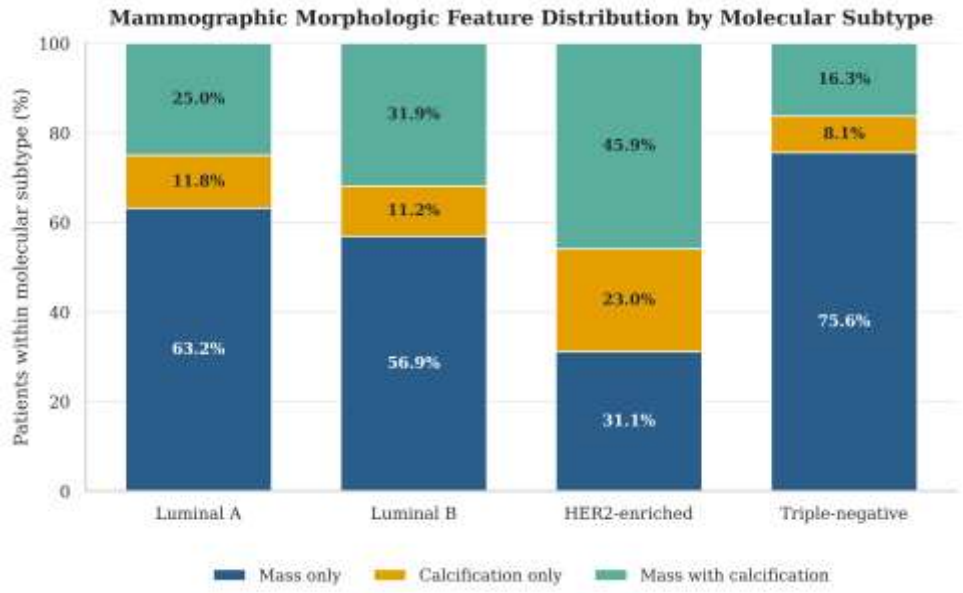

Figure 2 Distribution of Mammographic Morphologic Features Across Molecular Subtypes

Note. Percentages are calculated within each molecular subtype and sum to 100% within each bar.

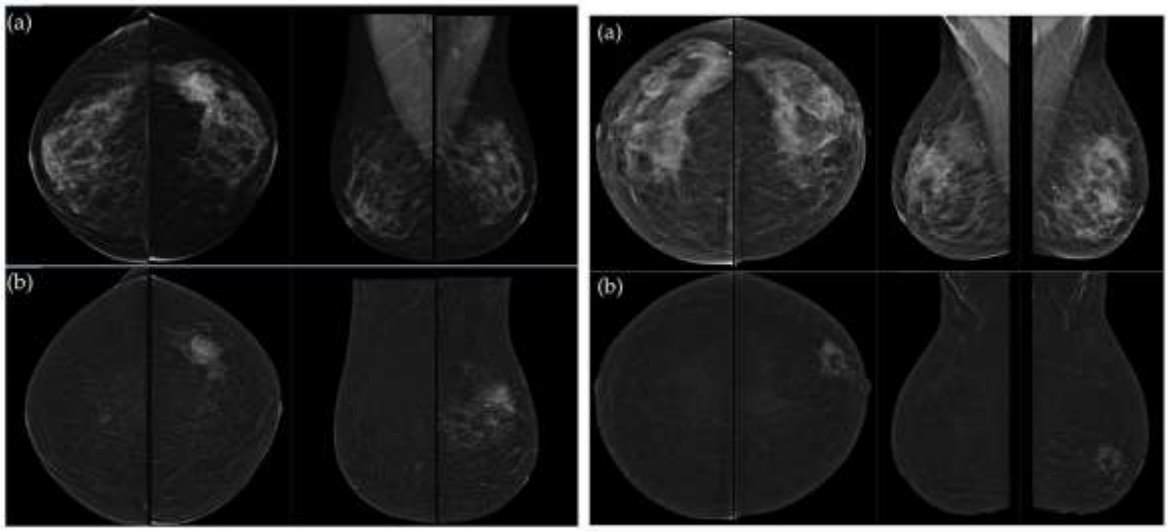

Figure 3 Illustrative Contrast-Enhanced Mammography Cases of HER2-Enriched and Triple-Negative Breast Cancer

Note. These radiographs are illustrative published cases and are not participants from the present CMMD cohort. Top: HER2-enriched breast carcinoma; low-energy craniocaudal and mediolateral oblique views show focal asymmetry with suspicious microcalcifications, while recombined images show a large heterogeneous enhancing area. Bottom: triple-negative breast carcinoma; low-energy views show a relatively well-circumscribed round-to-oval mass without suspicious calcifications, while recombined images show rim enhancement with heterogeneous internal uptake. Reproduced from Figures 5 and 6 in Ferenčaba et al. (2026) under the Creative Commons Attribution 4.0 International license (https://creativecommons.org/licenses/by/4.0/).

The primary chi-square analysis rejected the null hypothesis of independence between morphologic feature and molecular subtype (chi-square[6] = 52.72, P < .001). All expected cell counts exceeded 11, satisfying the large-sample assumption. The overall association was small-to-moderate in magnitude (Cramer's V = .188, 95% bootstrap CI [.150, .242]). Adjusted standardized residuals identified HER2-enriched mass-only presentation as markedly less frequent than expected (residual = -6.35), while HER2-enriched calcification-only and mass-with-calcification presentations were more frequent than expected

(residuals = 3.76 and 4.07, respectively). Triple-negative mass-only presentation was more frequent than expected (residual = 3.95), whereas triple-negative mass with calcification was less frequent than expected (residual = -3.18). These cell-specific contributions are shown in Figure 4.

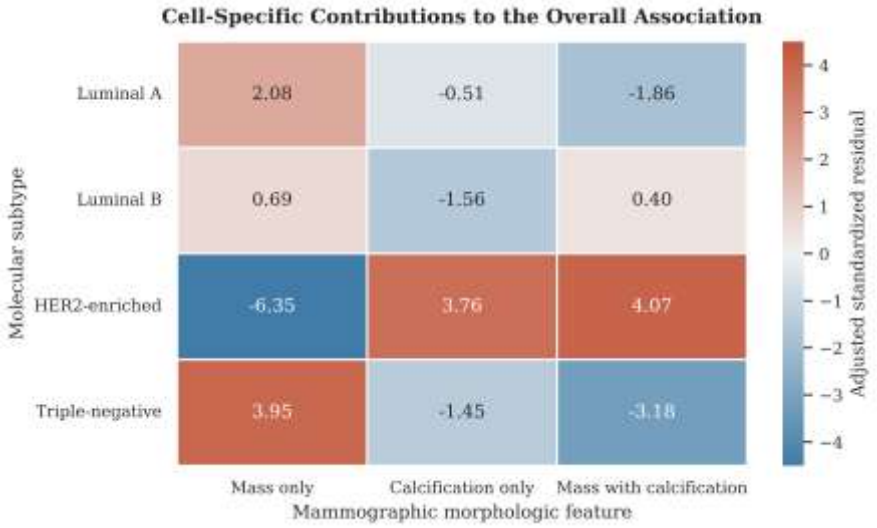

Figure 4 Adjusted Standardized Residuals for the Feature-by-Subtype Table

Note. Positive residuals indicate more observations than expected under independence; negative residuals indicate fewer. Absolute values near or above 2 identify influential cells.

Adjusted and Secondary Associations

After adjustment for age and laterality, the abnormality type also contributed significantly to molecular subtype in the adjusted multinomial model (likelihood-ratio chi-square[6] = 55.34, P < .001). All model estimates are shown in Table 3 and the feature-related RRRs are shown in Figure 5. Relative to luminal A and mass-only presentation, HER2-enriched cancer was 3.72 times as likely to occur in the mass-with-calcification category (RRR = 3.72, 95% CI [2.16, 6.41], P < .001) and 3.85 times as likely in the calcification-only category (RRR = 3.85, 95% CI [1.93, 7.68], P < .001). In both of the two categories of calcification, there was no significant association with luminal B vs luminal A. The RRRs for triple-negative cancer were both less than 1.00 but confidence intervals contained the null value. Laterality was not related to any subtype contrast, while there was a negative association between each 10-year increase in age and luminal B (RRR = 0.84, 95% CI [0.70, 0.99], P = .043) and triple-negative cancer (RRR = 0.77, 95% CI [0.60, 0.99], P = .039) compared to luminal A. The model converged and there were no empty cells or cells with unanticipated data.

Table 3 Multinomial Logistic Regression of Molecular Subtype

Outcome vs luminal A	Predictor	RRR	95% CI	P
Luminal B	Mass with calcification vs mass only	1.41	[0.91, 2.18]	.126
Luminal B	Calcification only vs mass only	0.94	[0.51, 1.74]	.849
Luminal B	Age, per 10 years	0.84	[0.70, 0.99]	.043
Luminal B	Right vs left breast	1.21	[0.83, 1.77]	.320
HER2-enriched	Mass with calcification vs mass only	3.72	[2.16, 6.41]	<.001
HER2-enriched	Calcification only vs mass only	3.85	[1.93, 7.68]	<.001
HER2-enriched	Age, per 10 years	0.97	[0.78, 1.19]	.743

Outcome vs luminal A	Predictor	RRR	95% CI	P
HER2-enriched	Right vs left breast	0.97	[0.60, 1.56]	.903
Triple-negative	Mass with calcification vs mass only	0.54	[0.27, 1.08]	.079
Triple-negative	Calcification only vs mass only	0.49	[0.19, 1.27]	.144
Triple-negative	Age, per 10 years	0.77	[0.60, 0.99]	.039
Triple-negative	Right vs left breast	0.80	[0.47, 1.37]	.416

Note. The reference outcome is luminal A; the reference feature is mass-only presentation. Estimates are adjusted for age and laterality and use Huber-White sandwich confidence intervals. CI = confidence interval; RRR = relative risk ratio. Overall likelihood-ratio chi-square(6) for abnormality type = 55.34, P < .001.

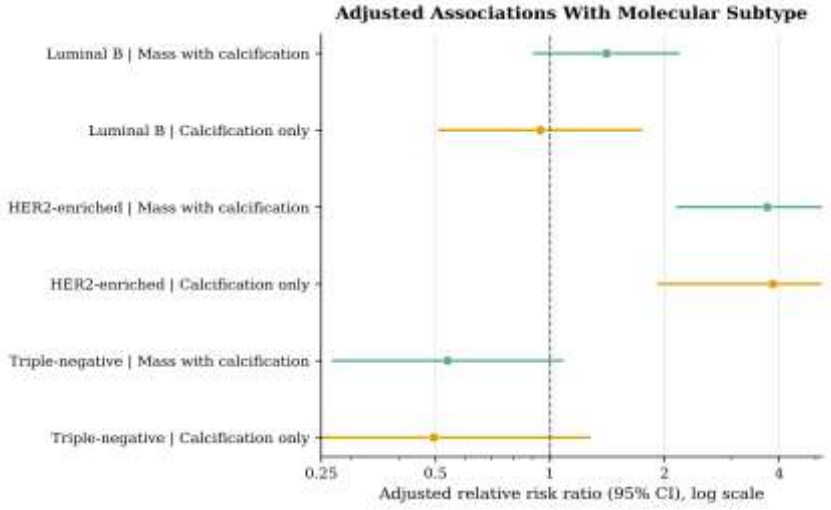

Figure 5 Adjusted Relative Risk Ratios for Morphologic Features and Molecular Subtype

Note. Luminal A is the reference outcome and mass-only presentation is the reference feature. Estimates are adjusted for age and breast laterality. CI = confidence interval; RRR = relative risk ratio.

The prespecified binary contrasts supported both directional hypotheses (Table 4). After adjustment for age and laterality, the prevalence of HER2-enriched cancer was 2.82 times higher among calcification-containing presentations than among mass-only presentations (adjusted PR = 2.82, 95% CI [2.01, 3.94], false-discovery-rate-adjusted P < .001). The prevalence of triple-negative cancer was 2.52 times higher among mass-only presentations than among calcification-containing presentations (adjusted PR = 2.52, 95% CI [1.57, 4.05], adjusted P < .001). In sensitivity analysis, combining luminal A and luminal B produced an adjusted luminal prevalence ratio of 0.82 for calcification-only versus mass-only presentation (95% CI [0.70, 0.98], P = .026); the estimate for mass with calcification was 0.91 (95% CI [0.82, 1.01], P = .073). These results were directionally consistent with greater concentration of calcification-containing findings in the HER2-enriched group.

Table 4 Prespecified Secondary Modified Poisson Contrasts

Outcome contrast	Feature contrast	Adjusted PR	95% CI	FDR-adjusted P
HER2-enriched vs other subtypes	Calcification-containing vs mass only	2.82	[2.01, 3.94]	<.001
Triple-negative vs other subtypes	Mass only vs calcification-containing	2.52	[1.57, 4.05]	<.001

Note. Models are adjusted for age and laterality. Benjamini-Hochberg correction was applied across the two prespecified secondary tests. CI = confidence interval; FDR = false discovery rate; PR = prevalence ratio.

Discussion

The results of this cross-sectional analysis showed a statistically significant correlation between simple morphologic features on mammograms and molecular subtype of breast cancer. The main hypothesis was confirmed as the distribution of presentations, mass only, calcification only and mass with calcification was not independent of molecular subtype. The overall effect size was small to moderate but the pattern of effects was different between the cells. Triple-negative cancers were relatively depleted from the calcification-containing categories and HER2-enriched cancers were relatively enriched in both categories of calcification. These relationships remained after taking into account age and laterality and were corroborated in prespecified binary contrasts. Therefore, the analysis answered the research question, both at the distributional and adjusted levels and demonstrated that the discriminative signal was the one mainly supported by the HER2-enriched and triple-negative phenotypes.

The HER2-enriched pattern is very similar to previous mammographic and CEM evidence. Davis et al. (2019) reported that calcifications and "extensive disease" are imaging features that are seen again and again in tumors that are HER2-enriched. Wang et al. (2022) reported a higher prevalence of calcification in the HER2-enriched group in a two-centre CEM study and non-mass enhancement was an independent predictor of that group. Ping et al. (2026) more recently found that 61.9% of the lesions that were HER2-overexpressing showed internal calcification and that the HER2-overexpressing lesions were most commonly non-mass. This is corroborated in the current study with a larger, open patient-level cohort, where 68.9% of the HER2-enriched cases did show calcification, and adjusted RRRs were >3.7 in both the calcification-only and the combined presentations when compared to luminal A mass-only disease. The observation of an agreement between the CEM and conventional morphology cohorts indicates that the imaging signal associated with HER2 does not occur only in the post-contrast period. It is also seen in the structural low-energy domain, but at present the available data do not indicate whether this is due to morphology and/or enhancement.

The triple-negative results were also consistent with previous studies. The prevalence of triple-negative disease was more than double among mass-only presentations compared with calcification-containing presentations and three-quarters of the triple-negative cancers in CMMD were mass-only. Johnson et al. (2021) described TNBC as frequently presenting as a non-calcified round or oval mass, often with circumscribed or indistinct margins, which were also observed in mammographic subtype comparisons (Sohn et al., 2016). Ping et al. (2026) indicated the mass-type appearance in 91.3% of triple-negative lesions, in addition to common oval morphology and rim enhancement. The shape, margin and enhancement are not included in the coding of the CMMD variable and the present result is only for the broad structural component of this phenotype. However, the strongly positive residuals of mass-only triple-negative presentation and low frequency of associated calcification are in line with the known imaging pattern.

Available features were a poorer discriminator of the luminal groups. Both luminal A and luminal B cancers were mainly mass-forming and there was no significant difference between the feature-related adjusted RRRs. An overlap is desirable because it helps to avoid false individual conclusions due to a statistically significant global association. Luminal subtyping is partly based on thresholds for proliferation and receptor-expression that may not result in large differences between the different luminal subtypes (Prat et al., 2015; Tang & Tse, 2016). Sensitivity analysis indicated a reduced prevalence of combined luminal disease in the calcification-only group, which was small and the lower bound of the confidence interval was close to the null for mass with calcification. In fact, imaging features should be interpreted as probabilistic correlates and not substitutes for the immunohistochemical classification.

The results also help to better understand the relationship between simple semantic morphology and more advanced CEM and artificial-intelligence research. Ma et al. (2025) discovered that models fused with the two types of images (low-energy and dual-energy subtraction) achieved better performance than models based on a single image type, demonstrating that the two image modalities provide complementary information. Radiomic analyses of CEM images have been able to identify quantitative signals to differentiate receptor-defined groups, tumor grade and TNBC (Marino et al., 2020; Nicosia et al., 2022; Zhang et al., 2021; Zhu et al., 2024) and deep-learning models based on mammography have been able to extract more information beyond the manually recorded subtypes (Luo et al., 2025; Mota et al., 2024). In the present study, the modest Cramer's V is similar to

that literature: mass and calcification categories truly do have biological content, but the coarseness of the categories means that there are also significant within-subtype variations. While a high-dimensional model could lead to better prediction, it is still important to determine the transparent association estimates that support the predictive performance, in order to identify which observable patterns underpin the prediction.

From a clinical point of view, the observed trends could guide radiologists in their pre-biopsy expectations and in exploring imaging-pathology discordance. A presentation with calcification was significantly enriched for HER2-enriched disease while a presentation without calcification was significantly enriched for triple-negative disease. These associations can support careful assessment of receptor status or resampling if the pathological findings are not in keeping with the overall imaging picture. They should not be used for the assignment of therapy or as a substitute for ER, PR, HER2 and Ki-67 testing. Imaging and pathology information is complementary and there was overlap across the feature categories and none of the morphologic presentations was unique for any of the individual subtypes (Harbeck et al., 2019; Johnson et al., 2021).

A number of features enhance the study. The analytical sample was larger than many published CEM subtype cohorts, the unit of analysis was the patient, not the individual view, and 100% of the primary variables were complete. The analysis included global association, effect size, bootstrap confidence interval for the effect size, cell-specific residuals, multinomial estimates that adjusted for the covariates, prespecified comparisons of prevalence ratios, and sensitivity analysis. An open dataset and recoding rules (made explicit) also facilitate reproducibility. More importantly, the study did not classify the conventional mammograms as contrast-enhanced mammograms, but instead recognized the exposure as the low-energy-equivalent morphologic domain (LEED), and used this domain throughout the analysis of the study.

The main constraint is the result of this design decision. The low-energy and recombined post-contrast CEM acquisitions (paired) are not included in CMMD. Hence, it is not possible to analyze enhancement intensity, distribution, internal enhancement pattern, background parenchymal enhancement or temporal contrast behavior. The fixed title should therefore only be interpreted in the light of the explicit operational definition that is provided in the methodology; the results only concern the structural morphology relevant to CEM. Second, the abnormality variable is coarse and does not consider BI-RADS features such as mass shape, margin, calcification morphology, calcification distribution, breast density or size of the lesion. Third, the raw ER, PR, HER2 and Ki-67 values were not reported in the public file, which means that they would not be available for reclassification based on other subtype definitions. Fourth, 1,316 malignant clinical records were only partially labelled with subtypes, 749 of which were labelled. This reflects the branch of this database that contains molecular-subtype data, but selection into this branch may be a limitation on generalizability. Finally, unknown potential confounding variables and/or effect modifiers include the acquisition center, menopausal status, and histologic grade and density. Lastly, the lack of external validation and the retrospective single-country cohort design restricts the transportability of the results, and the cross-sectional study design does not allow causal inferences.

These estimates must be confirmed in future studies with true paired acquisitions in CEM, standardized BI-RADS descriptors, receptor-level pathological findings and clinically relevant covariates. A valuable next step would be hierarchical modeling, first quantifying interpretable low-energy morphology, and then testing the added value of combining and enhancing images and testing radiomics as an additional step. Before making a clinical prediction claim, consider external validation, including calibration, subgroup performance and decision utility. Such work would clarify the potential of transparent association as employed here to provide strong imaging-based phenotyping while not over-emphasizing the role of imaging in molecular diagnosis.

CONCLUSION

This patient-level cross-sectional analysis showed a relationship between mammographic mass pattern and calcification pattern and molecular subtype. The number of HER2-enriched cancers was far greater in the calcification-containing presentations and triple-negative cancers were concentrated in the mass-only presentations; both associations were present after controlling for age and laterality. The results thus confirmed the primary and directional hypotheses and illustrated that measurable information is present in simple structural morphology that is related to subtype. But due to the moderate effect size and the significant overlap between groups, it is not possible to deterministically classify subtypes. The evidence is relevant to CMMD, which does not contain recombined post-contrast images, and thus applies only to the low-energy-equivalent morphologic component relevant to CEM and not to enhancement behavior. These features may be used in addition to pathological evaluation, and may encourage more thorough study of CEM; but receptor testing is still the key determinant of treatment decisions.

REFERENCES

[1] Bray, F., Laversanne, M., Sung, H., Ferlay, J., Siegel, R. L., Soerjomataram, I., & Jemal, A. (2024). Global cancer statistics 2022: GLOBOCAN estimates of incidence and mortality worldwide for 36 cancers in 185 countries. *CA: A Cancer Journal for Clinicians*, *74*(3), 229–263. https://doi.org/10.3322/caac.21834

[2] Cai, H., Wang, J., Dan, T., Li, J., Fan, Z., Yi, W., Cui, C., & Li, L. (2023). An online mammography database with biopsy confirmed types. *Scientific Data*, *10*, 123. https://doi.org/10.1038/s41597-023-02025-1

[3] Covington, M. F., Pizzitola, V. J., Lorans, R., Weaver, B. D., & Fajardo, L. L. (2024). State-of-the-art for contrast-enhanced mammography. *British Journal of Radiology*, *97*(1156), 695–704. https://doi.org/10.1093/bjr/tqae017

[4] Ferenčaba, A. O., Galić, D., Ivanac, G., Kralik, K., Smolić, M., Steiner, J., Pedišić, I., & Bojanic, K. (2026). Contrast-enhanced mammography and deep learning-derived malignancy scoring in breast cancer molecular subtype assessment. Medicina, 62(1), 115. https://doi.org/10.3390/medicina62010115

[5] Francescone, M. A., Jochelson, M. S., Dershaw, D. D., Sung, J. S., Hughes, M. C., Zheng, J., Moskowitz, C., & Morris, E. A. (2014). Low energy mammogram obtained in contrast-enhanced digital mammography is comparable to routine full-field digital mammography. *European Journal of Radiology*, *83*(8), 1350–1355. https://doi.org/10.1016/j.ejrad.2014.05.015

[6] Harbeck, N., Penault-Llorca, F., Cortes, J., Gnant, M., Houssami, N., Poortmans, P., Ruddy, K., Tsang, J., & Cardoso, F. (2019). Breast cancer. *Nature Reviews Disease Primers*, *5*, 66. https://doi.org/10.1038/s41572-019-0111-2

[7] Jochelson, M. S., & Lobbes, M. B. I. (2021). Contrast-enhanced mammography: State of the art. *Radiology*, *299*(1), 36–48. https://doi.org/10.1148/radiol.2021201948

[8] Johnson, K. S., Conant, E. F., & Soo, M. S. (2021). Molecular subtypes of breast cancer: A review for breast radiologists. *Journal of Breast Imaging*, *3*(1), 12–24. https://doi.org/10.1093/jbi/wbaa110

[9] Luo, Y., Wei, J., Gu, Y., Zhu, C., & Xu, F. (2025). Predicting molecular subtype in breast cancer using deep learning on mammography images. *Frontiers in Oncology*, *15*, 1638212. https://doi.org/10.3389/fonc.2025.1638212

[10] Ma, M., Xu, W., Yang, J., Zheng, B., Wen, C., Wang, S., Xu, Z., Qin, G., & Chen, W. (2025). Contrast-enhanced mammography-based interpretable machine learning model for the prediction of the molecular subtype breast cancers. *BMC Medical Imaging*, *25*, 255. https://doi.org/10.1186/s12880-025-01765-3

[11] Marino, M. A., Pinker, K., Leithner, D., Sung, J., Avendano, D., Morris, E. A., Jochelson, M. S., & Thakur, S. B. (2020). Contrast-enhanced mammography and radiomics analysis for noninvasive breast cancer characterization: Initial results. *Molecular Imaging and Biology*, *22*(3), 780–787. https://doi.org/10.1007/s11307-019-01423-5

[12] Mota, A. M., Mendes, J., & Matela, N. (2024). Breast cancer molecular subtype prediction: A mammography-based AI approach. *Biomedicines*, *12*(6), 1371. https://doi.org/10.3390/biomedicines12061371

[13] Nguyen, M. T. H., Varma, N., Cheong Wah, D. L., Chew, R., Botha, T., Kouloyan-Ilic, S., & Paiva, J. (2024). Performance of contrast-enhanced mammography for detecting multifocal and multicentric breast cancer and evaluating tumour size, and implications for surgical management: Early experience in a tertiary centre. *Journal of Medical Imaging and Radiation Oncology*, *68*(2), 141–149. https://doi.org/10.1111/1754-9485.13616

[14] Nicosia, L., Bozzini, A. C., Ballerini, D., Palma, S., Pesapane, F., Raimondi, S., Gaeta, A., Bellerba, F., Origgi, D., De Marco, P., Castiglione Minischetti, G., Sangalli, C., Meneghetti, L., Curigliano, G., & Cassano, E. (2022). Radiomic features applied to contrast enhancement spectral mammography: Possibility to predict breast cancer molecular subtypes in a non-invasive manner. *International Journal of Molecular Sciences*, *23*(23), 15322. https://doi.org/10.3390/ijms232315322

[15] Phillips, J., Mehta, T. S., Portnow, L. H., Fishman, M. D. C., Zhang, Z., & Pisano, E. D. (2023). Comparison of contrast-enhanced mammography with MRI utilizing an enriched reader study: A breast cancer study (CONTRRAST trial). *Radiology*, *309*(2), e230530. https://doi.org/10.1148/radiol.230530

[16] Ping, Y., Li, Y., Qu, T., Qin, Y., Zhao, Y., Shi, B., Rong, X., Wang, H., Wang, T., Zhang, J., & Xue, J. (2026). Contrast-enhanced mammography based quantitative and qualitative feature analysis across different breast cancer molecular subtypes. *Cancer Imaging*, *26*, 18. https://doi.org/10.1186/s40644-025-00979-6

[17] Polat, D. S., Evans, W. P., & Dogan, B. E. (2020). Contrast-enhanced digital mammography: Technique, clinical applications, and pitfalls. *American Journal of Roentgenology*, *215*(5), 1267–1278. https://doi.org/10.2214/AJR.19.22412

[18] Prat, A., Pineda, E., Adamo, B., Galván, P., Fernández, A., Gaba, L., Díez, M., Viladot, M., Arance, A., & Muñoz, M. (2015). Clinical implications of the intrinsic molecular subtypes of breast cancer. *The Breast*, *24*(Suppl. 2), S26–S35. https://doi.org/10.1016/j.breast.2015.07.008

[19] Sohn, Y. M., Han, K., & Seo, M. (2016). Immunohistochemical subtypes of breast cancer: Correlation with clinicopathological and radiological factors. *Iranian Journal of Radiology*, *13*(4), e31386. https://doi.org/10.5812/iranjradiol.31386

[20] Tang, P., & Tse, G. M. (2016). Immunohistochemical surrogates for molecular classification of breast carcinoma: A 2015 update. *Archives of Pathology & Laboratory Medicine*, *140*(8), 806–814. https://doi.org/10.5858/arpa.2015-0133-RA

[21] von Elm, E., Altman, D. G., Egger, M., Pocock, S. J., Gøtzsche, P. C., & Vandenbroucke, J. P. (2007). The Strengthening the Reporting of Observational Studies in Epidemiology (STROBE) statement: Guidelines for reporting observational studies. *The Lancet*, *370*(9596), 1453–1457. https://doi.org/10.1016/S0140-6736(07)61602-X

[22] Wang, S., Wang, Z., Li, R., You, C., Mao, N., Jiang, T., Wang, Z., Xie, H., & Gu, Y. (2022). Association between quantitative and qualitative image features of contrast-enhanced mammography and molecular subtypes of breast cancer. *Quantitative Imaging in Medicine and Surgery*, *12*(2), 1270–1280. https://doi.org/10.21037/qims-21-589

[23] Zhang, Y., Liu, F., Zhang, H., Ma, H., Sun, J., Zhang, R., Song, L., & Shi, H. (2021). Diagnostic value of radiomics analysis in contrast-enhanced spectral mammography for identifying triple-negative breast cancer. *Frontiers in Oncology*, *11*, 773196. https://doi.org/10.3389/fonc.2021.773196

[24] Zhu, S., Wang, S., Guo, S., Wu, R., Zhang, J., Kong, M., Pan, L., Gu, Y., & Yu, S. (2024). Contrast-enhanced mammography radiomics analysis for preoperative prediction of breast cancer molecular subtypes. *Academic Radiology*, *31*(6), 2228–2238. https://doi.org/10.1016/j.acra.2023.12.005

[25] Zou, G. (2004). A modified Poisson regression approach to prospective studies with binary data. *American Journal of Epidemiology*, *159*(7), 702–706. https://doi.org/10.1093/aje/kwh090